Two Clusters of Charged Residues Located in the Electropositive Face of the Von Willebrand Factor A1 Domain Are Essential for Heparin Binding†

Ghassem Rastegar-Lari,‡ Bruno O. Villoutreix,§ Anne-Sophie Ribba,‡ Paulette Legendre,‡ Dominique Meyer,‡ and Dominique Baruch*,‡

INSERM U143, Bicetre, and INSERM U428, Paris, France

Received January 16, 2002; Revised Manuscript Received March 13, 2002

ABSTRACT: The VWF A1 domain seems to possess two heparin binding regions (residues 565−587 and 633−648) displaying positively charged amino acids, but the overall polyanion−A1 domain interaction scheme remains essentially elusive. To probe this molecular reaction as well as the role of electrostatic forces in VWF−heparin interaction, we performed mutagenesis and molecular modeling experiments. Fifteen mutated rVWFs were expressed [R571A, K572A, R573A, K585A, R571A/K572A/R573A, R578A/R579A, R578A/R579A/K585A, R571A/K572A/R573A/R578A/R579A/K585A (6A), K642G, K643G, K644G, K645G, K642G/K645G, K643G/K644G, and K642G/K643G/K644G/K645G (4G)]. Experimental results indicate that the multimeric structure of the mutants was similar to that of wild-type (WT) rVWF and that all rVWFs displayed normal binding to four conformation-dependent mAbs directed against the A1 domain. Three variants displayed significant reductions in the level of heparin binding. The 6A variant showed 39.2 ± 1.3% of the WT rVWF level ($p < 0.005$), while mutants K643G/K644G and 4G showed 63.6 ± 3.2 and 53.3 ± 5% of the WT rVWF level, respectively ($p < 0.005$). Computational investigations showed that one face of the A1 domain is strongly electropositive, indicating that electrostatic forces should be essential in steering heparin onto its binding site. In agreement with our experimental data, the most striking alterations of the electrostatic potential contours were seen for mutants 4G, K643G/K644G, and 6A. Our data suggest that two clusters, one at positions 571−573, 578, 579, and 585 and the other at positions 642−645, act in concert for the recognition of heparin, forming a single extended binding surface across the electropositive face of the VWF A1 domain. A structural model of the VWF A1 domain−heparin complex is proposed, taking into account both experimental and computer modeling data.

Von Willebrand factor (VWF)[1] is a multimeric protein that performs essential functions in hemostasis as a carrier of coagulation factor VIII in plasma, and as a ligand for primary platelet adhesion at sites of vascular damage. Although circulating VWF does not normally interact with platelets, the presence of high shear forces induces an interaction between platelets and plasma or subendothelial VWF. This leads to platelet adhesion and activation and subsequently thrombus formation. VWF consists of disulfide-linked multimers formed of 250 kDa subunits. Each subunit contains four types of repeated domains, in the order D′, D3, A1, A2, A3, D4, C1, C2, and CK. The A1 and A3 domains carry most functional binding sites for the platelet receptor GPIb, and for collagen molecules, whereas C1 contains the GPIIb-IIIa recognition site (*1*). Heparin has been suggested to modulate GPIb−VWF interactions in a yet unresolved fashion, leading to either an inhibition or an improvement in the latter interaction (*2*, *3*). Electrostatic forces have been found to be essential (in numerous situations, but not in all cases) for protein interactions with heparin, a negatively charged polymer of a regular disaccharide repeat sequence (α-1,4-L-iduronic acid → D-glucosamine) with a high degree of sulfation (*4*). It is known that VWF−heparin interaction is very sensitive to salt concentration and that the minimal size of sulfated polysaccharide necessary to bind to VWF requires 18 monosaccharides (*5*, *6*). Previous studies have led to the identification of heparin binding sites within the A1 domain, while another site within the D′ domain was considered accessory, since a rVWF deleted of its A1 domain (ΔA1-rVWF) was unable to bind to heparin (*7*−*9*). Within the A1 domain of VWF, two sequences containing positively charged residues were deduced from alignment with heparin binding consensus sequences and homology modeling (*10*, *11*). However, peptide inhibition and mutagenesis studies have led to a profound discrepancy (*10*, *12*). Indeed, only the peptide extending between residues Tyr^{565} and Ala^{587}, and not the one encompassing the segment of Asn^{633}−Val^{648}, was able to bind to heparin (*10*). Within the former region, the mutation of a positively charged cluster within the segment of Tyr^{565}−Ala^{587} (Lys^{569}, Asp^{570}, Arg^{571}, Lys^{572}, and

† The work was funded in part by EC Grant BMH4-983517. G.R.-L. was supported by a doctoral fellowship from the Fondation pour la Recherche Medicale.

* To whom correspondence should be addressed: INSERM U143, 84 rue du General Leclerc, 94 276 Bicetre Cedex, France. Telephone: 33 1 49 59 56 28. Fax: 33 1 46 71 94 72. E-mail: baruch@kb.inserm.fr.

‡ INSERM U143.

§ INSERM U428.

[1] Abbreviations: VWF, Von Willebrand factor; rVWF, recombinant VWF; WT, wild-type; PBS, phosphate-buffered saline; BSA, bovine serum albumin; mAb, monoclonal antibody; SEM, standard error of the mean.

10.1021/bi020044f CCC: $22.00
Published on Web 05/02/2002

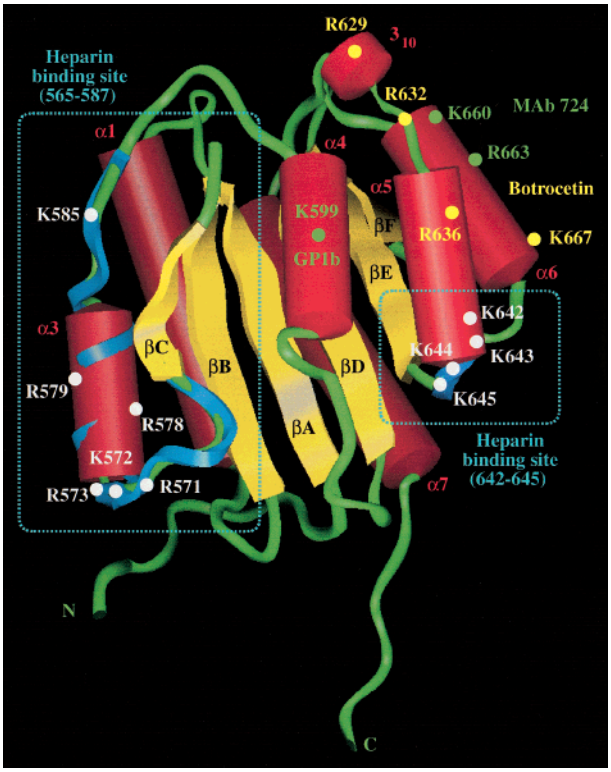

FIGURE 1: Three-dimensional secondary structure rendering of the VWF-A1 domain. Helices are shown as cylinders (red) and labeled α1−α7, while strands are marked *β*A−*β*F (nomenclature for the labeling follows that reported in ref *13*) and depicted as arrows (yellow). The loops connecting these segments are in green. N and C denote the N- and C-termini, respectively. One heparin binding site (residues 565−587) expands over part of the α3 helix, while the other (residues 642−645) is located after the α5 helix (a blue ribbon highlights these two sites). Alanine and glycine substitution mutants are shown in white. Botrocetin and mAb 724 binding sites are shown in yellow (Arg^{629}, Arg^{632}, Arg^{636}, and Lys^{667}) and green (Lys^{660} and Arg^{663}), respectively. A key residue (Lys^{599}) involved in GPIb binding is present on helix α4.

Arg^{573}) did not abrogate VWF binding to heparin−Sepharose beads. In contrast, mutating the cluster of four basic residues (Lys^{642}, Lys^{643}, Lys^{644}, and Lys^{645}) to Ala resulted in a severely impaired interaction (*12*). Therefore, we decided to investigate in detail the contribution to VWF−heparin interaction of basic residues located in both regions (Tyr^{565}−Ala^{587} and Lys^{642}−Lys^{645}).

The VWF A1 domain X-ray structure has so far been very valuable for the analysis of its residues involved in binding to GPIb or botrocetin, a snake venom protein that binds to VWF and improves its interaction with GPIb (*13*−*15*). The two putative heparin binding sites can readily be localized in the three-dimensional (3D) structure (see Figure 1), between residues Tyr^{565} and Ala^{587} over the α3 helix and as four consecutive lysine residues (Lys^{642}−Lys^{645}) in the C-terminal region of helix α5 for Lys^{642} and Lys^{643} and in the turn region next to helix α5 for Lys^{644} and Lys^{645} (*11*, *12*). Yet, despite this information, no structural model representing the interaction between heparin and the A1 domain has been proposed thus far, and there is a lack of a proposal explaining how the two molecules could bind to each other. We hypothesized that each positively charged cluster could be essential for heparin binding and that the two areas, separated by a distance of ∼25−30 Å, may act in concert for the recognition of heparin. Such binding properties of the VWF A1 domain would then be fully compatible with the required 18-mer heparin molecule necessary for the interaction and the observed inhibitory influence of salt. To clarify and rationalize the so far undefined molecular mechanisms leading to the formation of the A1 domain−heparin complex, the unknown overall 3D structure of the complex, and the possible role of electrostatic forces in this interaction, we decided to combine site-directed mutagenesis experiments and computational studies. To this end, we constructed eight mutants that included substitutions of six basic residues, alone or in combination, resulting in four single mutants and four clusters of charged-to-alanine residue substitutions. In addition, we constructed seven charged-to-neutral mutations of residues located on the surface of the A1 domain within the cluster of four lysines. As a complementary approach, we decided to substitute charged residues with glycine residues since this cluster was already analyzed following alanine replacement (*12*).

Our experimental results shed new light on the interaction of VWF with heparin, because they suggest for the first time that two positively charged clusters (one made up of Arg^{571}, Lys^{572}, Arg^{573}, Arg^{578}, Arg^{579}, and Lys^{585} and the other made up of Lys^{642}, Lys^{643}, Lys^{644}, and Lys^{645}) are necessary for optimal interaction. Furthermore, we show that individual substitution of these residues does not affect heparin binding, indicating that a set of weak electrostatic interactions spread over a relatively extended surface govern part of the molecular mechanism responsible for VWF−heparin interaction. Investigations of the electrostatic potentials ∼15 Å away from the molecular surface of the domain further address the molecular mechanism leading to the formation of the VWF−heparin complex as we noticed that one face of the A1 domain is essentially electropositive while the other tends to be electronegative. Overall, our functional approach associated with computer analysis of the wild-type (WT) and mutant structures allows us to propose the first approximate 3D model of this macromolecular complex.

EXPERIMENTAL PROCEDURES

Plasmids and Mutant Construction

Two plasmids contained the full-length cDNA of VWF (pSVVWFA and $pcDNA_3$VWF) and encoded wild-type rVWF (*16*, *17*). Nine plasmids containing mutated cDNA of VWF [pSVVWF-R571A, -K572A, -R573A, -K585A, -R578A/R579A, -R571A/K572A/R573A, -R578A/R579A/K585A, -R571A/K572A/R573A/R578A/R579A/K585A (6A), and -K642G/K643G/K644G/K645G (4G)], encoding the corresponding rVWF mutants, were constructed by site-directed mutagenesis using the QuickChange kit (Stratagene, La Jolla, CA) as previously described (*18*). Seven plasmids with mutated full-length cDNA ($pcDNA_3$-K642G, -K643G, -K644G, -K645G, -K642G/K645G, and -K643G/K644G), encoding the corresponding rVWF mutants, were obtained with the Transformer site-directed mutagenesis kit (Clontech, Palo Alto, CA) (*19*). Plasmids encoding substitution of alanine for lysine in position 660, of alanine for arginine in position 663, or alanine for lysine in position 667 were a kind gift from J. E. Sadler (Howard Hughes Medical Institute, St. Louis, MO) (*15*).

Transfection of Cells

Eighteen mutated rVWFs and WT rVWF were produced using the diethylaminoethyldextran method as previously described (*16*). Expression levels of COS-7 cells transfected with mutated and WT rVWF varied from 0.8 to 3 μg/mL. Conditioned medium from cells transfected with plasmid $pcDNA_3$ without full-length cDNA of VWF was used as negative control (mock-transfected cell medium). We also used ΔA1-rVWF obtained by stable expression in BHK cells (kind gift of J. J. Sixma, Department of Haematology, University Hospital, Utrecht, The Netherlands) (*20*).

Characterization of Antibodies and Radiolabeling of IgG

Monoclonal antibodies (mAbs) directed against human VWF were purified as IgGs (*21*). mAb 505, used for indirect labeling of rVWF in heparin and platelet binding assays, had its epitope located between amino acids 927 and 1114 (*22*). We have determined that mAb 505 interacts with all mutated rVWFs tested in this study, in a way similar to that with WT rVWF, and does not inhibit binding of rVWF to platelets or to heparin. mAbs 713 (epitope between residues 593 and 678), mAb 701 (overlapping residue 599), and mAb 328 (residues on either side of the disulfide loop of the A1 domain) have a conformation-dependent epitope against the A1 domain and inhibit binding of rVWF to platelets induced by ristocetin (*22*). mAb 724 also has a conformation-dependent epitope (including residues 660 and 663) and blocks VWF binding to botrocetin or to heparin (*23*). Rabbit anti-VWF polyclonal antibody (pAb) was prepared in the laboratory (*17*). Antibodies were labeled with $Na^{125}I$ (Amersham, Les Ulis, France) and Iodogen. The specific radioactivity varied from 1 to 4 μCi/μg. Labeled antibodies were stored at 4 °C and used within 1 month.

VWF Antigen Determination

The amount of VWF:Ag present in the conditioned medium after transfection was determined by an enzyme-linked immunoadsorbent assay (ELISA) using a pool of mAbs to VWF. Data were expressed in micrograms per milliliter. We verified that the binding of mAb 505 to mutated and WT rVWF, which was used for indirect labeling of rVWF, was similar to that of a pool of 35 mAbs.

Multimers and Subunit Analysis

The multimeric composition of rVWF was analyzed by 0.1% SDS−1% agarose gel electrophoresis under nonreducing conditions and stained with rabbit anti-VWF [^{125}I]pAb (*24*). In separate experiments, subunit analysis was performed under reducing conditions by electrophoresis on a 0.1% SDS−5% polyacrylamide gel followed by immunotransfer onto a nitrocellulose membranes and staining with rabbit anti-VWF [^{125}I]pAb (Bio-Rad, Marnes-la-Coquette, France) (*25*).

Binding of rVWF to mAbs

Binding to mAbs against the A1 domain of VWF was performed according to the method of Matsushita et al. (*15*), with some modifications. Briefly, wells of Maxi-sorp Nunc-Immuno plates (A/S Nunc, Roskilde, Denmark) were coated by incubating 200 μL of mAb 328, 701, 713, or 724 (5 μg/mL) in 50 mM carbonate buffer at pH 9.6 and 37 °C for 2 h. Wells were washed with phosphate-buffered saline (PBS) containing 0.1% Tween-20 (PBS/T) and blocked with 3% bovine serum albumin (BSA) (Calbiochem, La Jolla, CA) in PBS/T (1 h at 37 °C). Wells were incubated with various concentrations of WT or mutated rVWF in PBS/T containing 3% BSA (2 h at 37 °C). The wells were washed again and incubated with [^{125}I]pAb to VWF (5 ng/mL, 24 h at 4 °C). Wells were washed and dried, and the associated radioactivity was counted. The level of binding of mutated rVWF was determined and normalized to the value obtained for WT rVWF. Conditioned medium from cells transfected with plasmid $pcDNA_3$ without full-length cDNA of VWF was used as a negative control.

Heparin Binding Assay

Binding of mutated and WT rVWF to heparin−agarose beads was performed as previously reported (*26*). Samples of rVWF (100 μL) were diluted in mock-transfected cell medium so that final concentrations varied between 0.125 and 0.25 μg/mL, and the samples were preincubated for 30 min at 20 °C with a subsaturating amount of ^{125}I-labeled mAb 505 (5 ng/mL, $1-2 \times 10^4$ cpm, 50 μL) diluted in 20 mM Mes-Tris and 150 mM NaCl containing 0.5% BSA (*6*, *27*, *28*). Heparin (sodium salt, porcine intestinal mucosa, Sigma, La Verpillere, France) was immobilized on aminoethylagarose beads using a ratio of 60 mg of heparin to 1 g of aminoethylagarose beads, in most experiments, unless stated otherwise (ratio of 4 mg/g) (*6*). Heparin−agarose beads (100 μL) were added to the [^{125}I]mAb 505/rVWF mixture, and the mixture was incubated for 1 h at 20 °C. Duplicate aliquots (100 μL) were layered onto 200 μL of 25% sucrose in microfuge tubes and centrifuged for 3 min at 12000*g*, and the amount of bound ligand was counted as described previously (*26*). The level of nonspecific binding was determined for each data point using control agarose beads ($2 \pm 0.6\%$ for WT rVWF). Specific binding was calculated as total binding minus nonspecific binding.

Binding of rVWF to Platelets

Binding of rVWF to platelets was performed as described with few modifications (*27*). Washed platelets were prepared from outdated platelet concentrates by centrifugation at 200*g* for 15 min and fixed with paraformaldehyde (2%) in 0.15 mol/L NaCl and 25 mmol/L Tris-HCl buffer (pH 7.4) (TBS) containing 0.1% BSA. rVWF (0.25 μg/mL) diluted in TBS containing 1% BSA was preincubated with [^{125}I]mAb 505 (5 ng/mL) for 30 min at 20 °C. The final mixture contained 10^8 platelets/mL, [^{125}I]mAb 505−rVWF complexes, and 1 mg/mL ristocetin (Diagnostica Stago, Asnières, France) or 1 μg/mL botrocetin (kind gift of J. P. Girma, U143). After incubation for 1 h at 20 °C, duplicate aliquots (100 μL) were layered onto 200 μL of 25% sucrose in microfuge tubes and centrifuged for 3 min at 10000*g*. The tube tip containing the bound ligand was separated from the supernatant. Bound and free radioactivities were counted in a γ-counter (LKB Instruments SA, Bromma, Sweden). The percentage of total bound radioactivity was calculated as bound/(free + bound) radioactivity. Nonspecific binding was obtained by incubating platelets with [^{125}I]mAb 505 and ristocetin or botrocetin in the absence of rVWF. Specific binding was obtained by subtracting nonspecific binding from total binding. The

percentage of bound rVWF was normalized to the value obtained for WT rVWF.

Statistical Analysis

Mean values of percentages of heparin binding and their standard errors (SEM) were calculated from three experiments performed in duplicate. The statistical analysis was performed with Statview Software (Abacus Concepts, Berkeley, CA) using a Student's *t* test for unpaired samples, and a p value of <0.05 was considered significant.

Computational Approaches

Generating WT VWF and Variant Structural Models. The WT VWF A1 domain X-ray coordinates were obtained from the Protein Data Bank (*13*). One missing side chain was rebuilt using InsightII (Biopolymer module) software package version 2000 (Accelrys, San Diego, CA) running on a Silicon Graphics O2 R12000 workstation. X-ray water molecules were removed while the structure was solvated in a 20 Å layer of explicit water. These latter molecules were generated with the SOAK option of InsightII and have parameters that resemble those of the SPC and TIP3P water models (please see Accelrys User Guides). Explicit hydrogens were added, and lysine, arginine, histidine, aspartate, and glutamate residues were assumed to be charged. Energy minimization was performed with the new version of Discover and consistent valence force field (CVFF) parameters (Accelrys). A multiple-algorithm protocol for this process was used to relax the structure smoothly, thus avoiding a possible drastic departure from the initial X-ray conformation due, for example, to the addition of hydrogen atoms. The first step involved minimization of water molecules only. Then, protein heavy atoms were initially tethered to their experimental position with a force constant of 1 kcal mol^{-1} $Å^{-2}$, and the system was minimized using steepest descent and conjugate gradient. All restraints were progressively removed, and the system was finally minimized for 20 000 iterations. A dielectric constant of 1 was selected since explicit solvent molecules were present, together with a 25 Å nonbonded energy cutoff. With the X-ray structure as a starting point, amino acid substitutions mimicking the one introduced experimentally were carried out. Thus, 15 initial nonminimized structures were generated, then solvated, and energy minimized using the same protocol as for the WT protein.

Electrostatic Calculations and Rigid Body Docking. Electrostatic potential in solution under physiological ionic strength was calculated in and around the WT A1 domain and variants by means of a linear solution of the Poisson−Boltzmann equation using DelPhi version 98.0 (Accelrys) (*29*). The relaxed protein structures without the solvent molecules were positioned in the center of a grid box. The distance between the grid edges and the protein surface was at least 10 Å, and potentials at the boundary points were assigned according to Coulomb's law. This corresponds to positioning the protein in the center of grid with its largest dimension occupying ~50% of the grid length. Electrostatic potential was calculated at every point inside the grid. Also, to facilitate visualization of electrostatic potential 15 Å away from the molecular surface, a sphere was centered on the A1 domain's center of mass and color-coded according to the potential values. In our calculations, we set the internal dielectric constant to 4 and the outer dielectric constant to 80. The N- and C-termini were considered neutral, and formal charges were assigned to titratable residues. Default values for atomic radii were used.

An extended 18-mer heparin molecule was constructed using the NMR structure reported by Mulloy et al. (*30*). Heparin was docked interactively onto the WT A1 domain. In all situations, to reduce computational time, the polymer and the protein (no water molecules) were considered rigid. Initially, the polyanion was positioned along VWF regions of highest positive potential assuming the approach to be guided by electrostatic forces. More than 20 different orientations were generated. The heparin molecule was kept ~4 Å away from the protein surface, and for each position, the Coulombic interaction energy was calculated by adding the electrostatic contributions over all atoms of the two molecules. During these calculations, partial charges assigned during the energy minimization protocol for the protein or defined according to the CVFF parameters for heparin were applied. The contributions between atoms interacting with other atoms in the same molecule were ignored. The objective here was to evaluate interaction energies of many orientations of one molecule relative to the other, while searching for the orientations that resulted in low interaction energies.

RESULTS

Expression and Characterization of rVWF Mutants. To investigate the role of charged amino acids in heparin binding, we used site-directed mutagenesis to construct eight mutants in which positively charged amino acids within the VWF A1 domain of one heparin binding site (residues 565−587) were changed to alanine residues. In addition, we constructed seven mutants, with substitutions localized in the other heparin binding site of the A1 domain (residues 633−648), in which lysine residues were replaced with glycines (see the location in Figure 1). The corresponding mutated full-length cDNAs were transiently expressed in COS-7 cells. Each of the alanine or glycine substitution mutants exhibited secretion from COS-7 cells similar to that of WT rVWF (data not shown). The multimeric structure of each of the mutant proteins was similar to that of WT rVWF (data not shown). Each of the mutants proteins was secreted as full-length mature VWF (data not shown).

The reactivity of four conformation-dependent mAbs directed against distinct regions of the VWF A1 domain was tested toward the different rVWFs carrying mutated residues localized within the heparin binding sequences (residues 571−585 and 642−645). All rVWF mutants displayed binding to these mAbs similar to that of WT rVWF, indicating that the conformation of the A1 domain was not modified. Binding of the A1 domain in these 15 mutants was not impaired when using mAb 713 (Figure 2A) or mAb 724 (Figure 2B). In addition, we verified in the same experiment that mutant K660A, mutated within the epitope of mAb 724, displayed a complete lack of binding to mAb 724 while its binding to mAb 713 was close to that of the WT (Figure 2). Two other mAbs, mAb 701 and mAb 328, also known to be conformation-dependent and directed against the A1 domain, were screened for their reactivity toward the 15 mutants and found to interact normally with

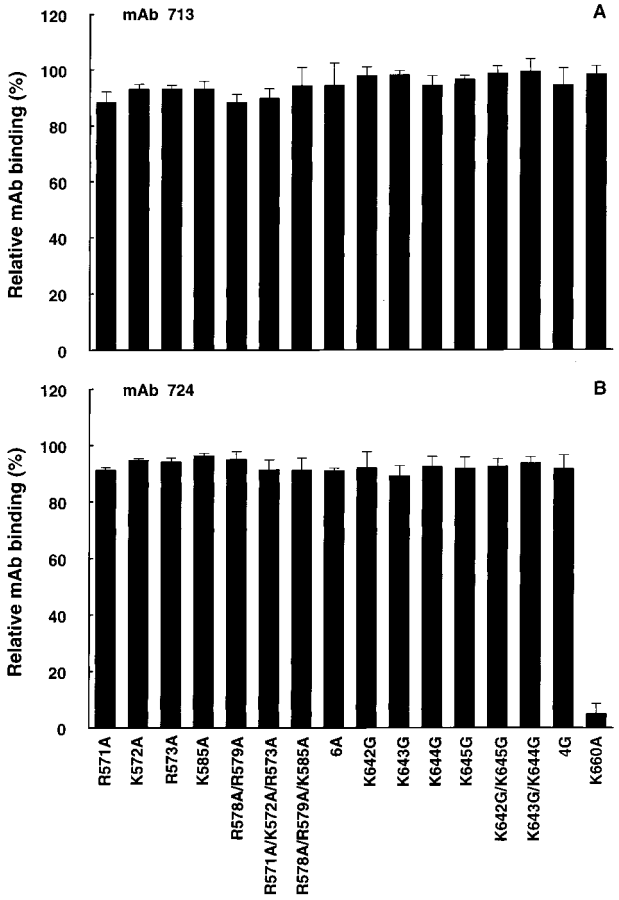

FIGURE 2: Binding of rVWF to conformation-dependent monoclonal antibodies against VWF. Wells coated with mAb 713 (A) or mAb 724 (B) were incubated with various concentrations of rVWF, and binding of rVWF was revealed by a radiolabeled polyclonal rabbit anti-VWF antibody. The level of binding of the mutants is expressed relative to the value obtained for WT rVWF. Each bar represents the mean ± SEM of three experiments performed in duplicate.

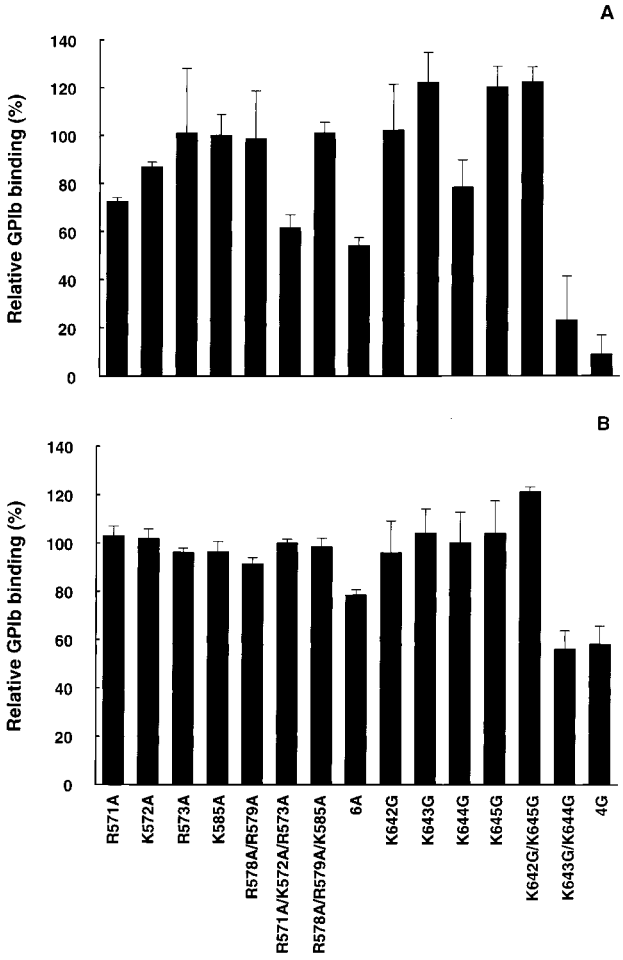

FIGURE 3: Histogram of VWF binding to GPIb. WT rVWF or mutated rVWF (0.25 μg/mL) labeled with [^{125}I]mAb 505 was incubated with paraformaldehyde-fixed platelets (10^8 per milliliter) for 1 h at room temperature, in the presence of ristocetin or botrocetin. Results were expressed as a percentage relative to that determined for WT rVWF. Results are from three experiments performed in duplicate (mean ± SEM). Binding to GPIb was induced by ristocetin (A) or botrocetin (B).

the mutated recombinant molecules (data not shown). Overall, this information indicates that the structural integrity of rVWF mutants was conserved and that these molecules could be used to probe heparin binding.

Binding of rVWF to GPIb. To characterize further the function of mutants, binding to platelet GPIb was assessed by quantitating the rVWF bound to formalin-fixed platelets in the presence of 1 mg/mL ristocetin (Figure 3A) or 1 μg/mL botrocetin (Figure 3B). The percentage of GPIb binding for each mutant protein was normalized to that obtained for WT rVWF. In the presence of ristocetin, three mutants (6A, K643G/K644G, and 4G) displayed binding to GPIb that was decreased by more than 50% compared to that of WT rVWF. In addition, the level of binding of R571A and R571A/R572A/R573A was slightly decreased (72.5 and 61.5% of that of WT rVWF, respectively). In addition, we found that at a low concentration of ristocetin (0.25 mg/mL), mutants R573A, R578A/R579A, and R578A/K579A/K585A showed increased levels of binding to GPIb that was 200% of that of WT (data not shown). This finding is in agreement with the fact that R578Q has been associated with a type 2B Von Willebrand disease (VWD) phenotype. 2B VWD is characterized by the ability of mutated VWF to bind platelet GPIb at lower ristocetin concentrations than normal VWF does (*31*). In the presence of botrocetin, each of the mutant proteins bound to platelets as well as WT rVWF with the exception of mutants K643G/K644G and 4G which bound at 56 and 58% of the level of maximal binding, respectively, whereas the level of binding of 6A reached 78.3% of that of WT rVWF (Figure 3B).

Binding of rVWF to Heparin. Binding of rVWF to heparin immobilized on agarose beads was assessed in the presence of [^{125}I]mAb to VWF used as a tracer. At rVWF concentrations between 0.1 and 0.25 μg/mL, the percentage of bound [^{125}I]mAb−rVWF complexes did not vary, reaching 35% of total radioactivity in the presence of WT. Interestingly, this level of binding did not exceed 16% in the presence of the 6A mutant ($p < 0.005$ for 6A vs WT). This indicates that the combined substitution of six charged residues resulted in a significant impairment of the ability of VWF to bind heparin. As a negative control, the level of binding of ΔA1-rVWF, deleted of its heparin binding site, to heparin−agarose beads did not exceed 5% of total radioactivity (Figure 4A).

To determine whether the binding of [^{125}I]mAb−rVWF complexes to heparin−agarose beads was specific, binding was performed in the presence of increasing soluble heparin

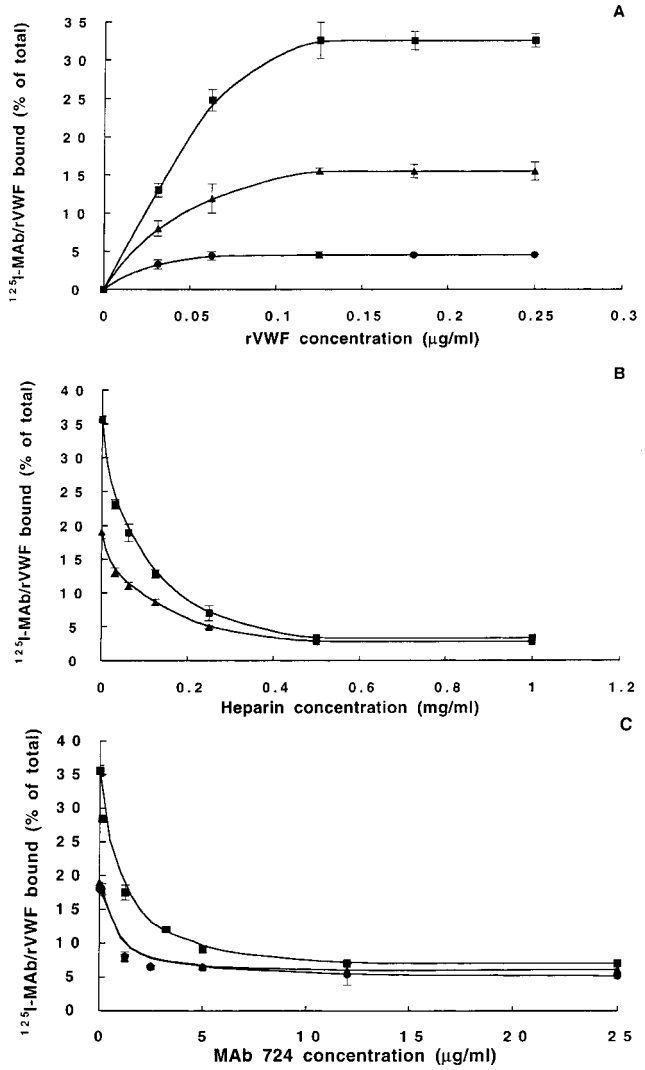

FIGURE 4: Binding of [^{125}I]mAb−WT rVWF and [^{125}I]mAb−6A rVWF complexes to heparin. Various concentrations of WT rVWF or mutants were preincubated with a subsaturating amount of [^{125}I]-mAb 505. Heparin−agarose beads were added to the radiolabeled mixture for 1 h. Bound ligand was separated from the supernatant by centrifugation, and bound radioactivity was counted and expressed relative to total radioactivity in the aliquot. (A) Comparison of WT rVWF (■), 6A-rVWF (▲), and ΔA1-rVWF (●) showing a plateau of ~35% binding in the samples containing WT rVWF, while 6A rVWF exhibited 16% binding. As a negative control, we used ΔA1-rVWF, with the heparin binding site deleted. (B) Inhibition of rVWF binding to heparin−agarose beads by soluble heparin. Heparin−agarose beads were added to the radiolabeled mixture in the presence of increasing concentrations of soluble heparin. Dose-dependent inhibition was obtained with IC_{50}s of 95 and 105 μg/mL, respectively, for WT rVWF (■) and 6A-rVWF (▲). The mean ± SEM was calculated from three independent measurements performed in duplicate. (C) Inhibition of rVWF binding to heparin−agarose beads by mAb 724. WT rVWF or mutants were preincubated with increasing concentrations of mAb 724, prior to the addition of heparin−agarose beads. The mean ± SEM was calculated from three independent measurements performed in duplicate: WT rVWF (■), 6A-rVWF (▲), and 4G-rVWF (●).

concentrations. A dose-dependent inhibition of [^{125}I]mAb−WT rVWF or [^{125}I]mAb−6A rVWF complexes binding to solid-phase heparin was observed (Figure 4B). The concentrations of soluble heparin required to inhibit 50% of the binding (IC_{50}) of WT and 6A rVWF to heparin−agarose

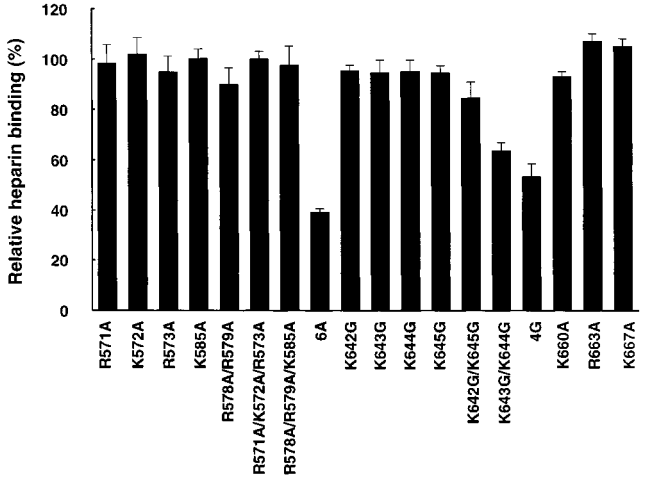

FIGURE 5: Histogram of rVWF mutants binding to heparin. The experimental procedure was as described in the legend of Figure 4. Binding of mutated rVWF to heparin−agarose beads was expressed as the percentage relative to that of WT rVWF. The mean ± SEM was calculated from three independent measurements performed in duplicate. rVWF mutants K643G/K644G, 6A, and 4G exhibited decreased levels of binding to heparin, as compared with WT rVWF ($p < 0.005$).

beads were 95 and 105 μg/mL, respectively. Addition of 1 mg/mL heparin reduced the level of [^{125}I]mAb−rVWF binding to the value observed when mock was used instead of WT rVWF or 6A rVWF. This result clearly demonstrates a competition between soluble and immobilized heparin for binding to rVWF. Finally, mAb 724, which was previously reported to block heparin binding to VWF, was assessed for its ability to inhibit heparin binding of different mutants. Complete inhibition of heparin binding to WT rVWF or the 6A or 4G mutant was reached in the presence of 5 μg/mL mAb 724 (Figure 4C). Taken together, these results show that the heparin binding assay used to assess the mutants is specific.

Figure 5 represents heparin binding of each rVWF alanine or glycine substitution mutant where the binding is expressed as a percentage of the maximal level of binding determined for WT rVWF. Alanine substitution mutants with a single, double, or triple mutation showed normal binding to heparin (90−102% of WT rVWF). In contrast, the level of binding of the 6A mutant was reduced to 39.2 ± 1.3% of that of the WT. Glycine substitution mutants with a single mutation showed binding levels of 94.4−95.3% of that of WT rVWF. Double mutants (K642G/K645G and K643G/K644G) and the mutant with the combined substitution of four glycine residues (4G) showed 84.5 ± 6.3, 63.6 ± 3.2, and 53.3 ± 5% heparin binding relative to that of WT rVWF, respectively. In addition, we obtained from J. E. Sadler three single rVWF mutants with the K660A, R663A, and K667A substitutions (*15*). These residues were found to form part of the epitope of the conformation-dependent anti-vWF mAb 724 or of the binding site of the VWF modulator botrocetin (*23*). We found that these three latter mutants exhibited normal heparin binding properties (93−107% heparin binding relative to that of WT rVWF). To determine whether a more complete reduction of binding could be obtained, we probed the mutants using smaller amounts of heparin immobilized on beads (4 vs 60 mg/g of beads). Under these conditions, 7% of the total radioactivity of mAb−rVWF

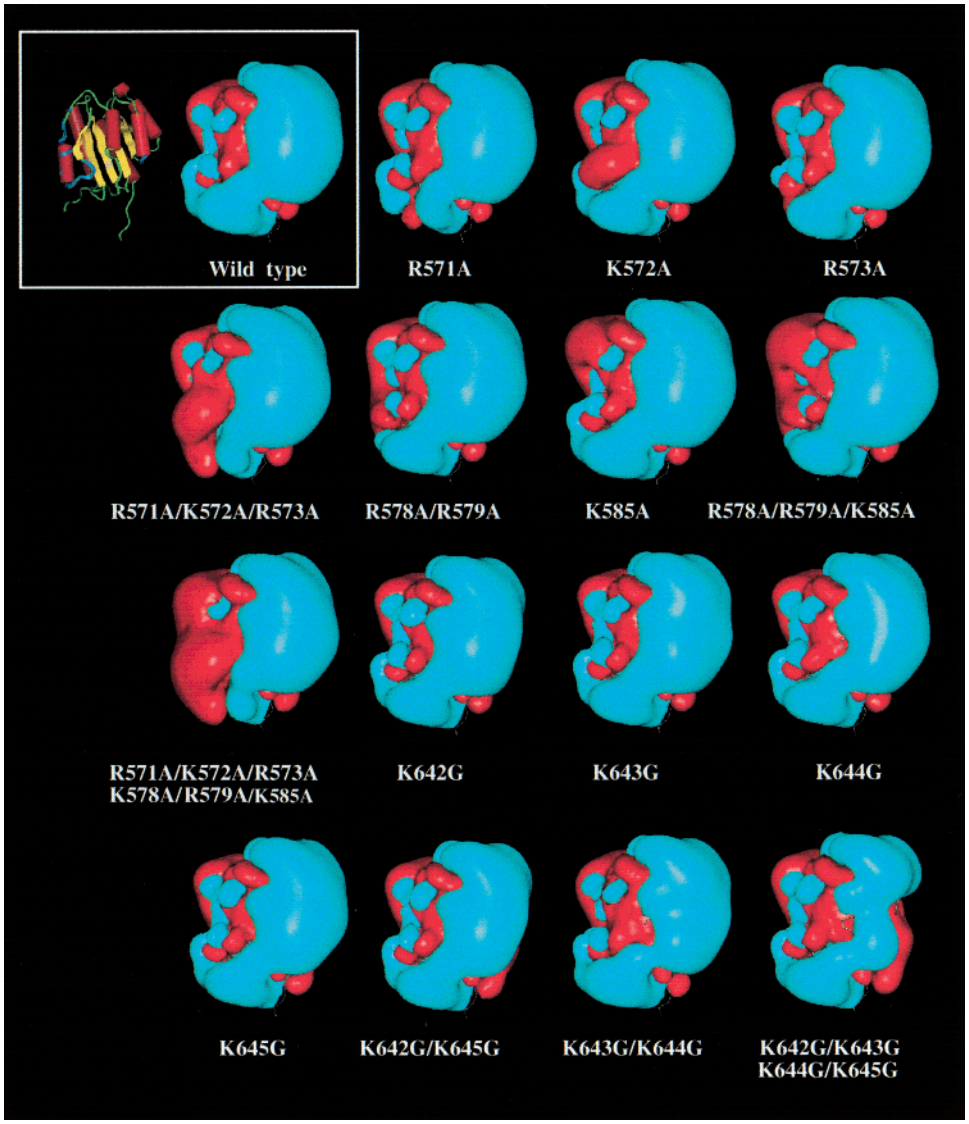

FIGURE 6: Three-dimensional isopotential contours of the WT VWF A1 domain and variants. Contours are at levels of −0.6 kT/e (red) and +0.6 kT/e (blue). They highlight the VWF A1 domain electrostatic potential asymmetry and illustrate the effect of some mutations on this energy field. Clearly, some substitutions alter significantly the electrostatic properties of the A1 domain (e.g., mutants 4G and 6A), while others (such as most single mutants) have little impact on the potentials (see the Results).

complexes is bound versus 35%. When the level of binding of the mutants was normalized to that of WT, we obtained 8, 49, 16, and 16% binding relative to that of WT for the 6A, K642G/K645G, K643/K644G, and 4G mutants, respectively. However, even under these conditions, none of the single mutants displayed a reduction in the level of binding.

Electrostatic Properties of WT and Mutant VWF Molecules. To compare some of the electrostatic properties of the WT and variant molecules, we modeled mutant proteins and refined their 3D structures with the same procedure to facilitate the comparative analysis. The root-mean-square deviation for backbone atoms between the initial A1 domain X-ray structure (PDB entry 1auq) and the relaxed WT and variant molecules was around 0.8−1.4 Å. As expected, small structural deviations with regard to the minimized X-ray conformation occurred in the vicinity of multiple-substitution regions. Electrostatic potentials were then calculated for all structures assuming the ionization state expected at neutral pH. First, because experimental data suggest that the interaction between the WT VWF A1 domain and heparin is dependent on electrostatic forces, we were interested in evaluating the potentials that were a relatively large distance from the molecular surface. Thus, the electrostatic potential values of WT VWF A1 domain were mapped on a virtual sphere, ∼15 Å from the molecular surface (data not shown). One face of the molecule is clearly electropositive, while the other face is definitively electronegative. Regions with strong electropositive character are readily identified via computation of isopotential contours (Figure 6). Clearly, such evaluations performed at moderate to high energy levels describe potentials some short distances away from the molecular surface. For the WT molecule, the areas strongly electropositive surround the N-terminus of the α3 helix and the C-termini of strand C and of helix 4 while also covering the α5, α6, and 3_{10} helices (see Figures 1 and 6). We expect that amino acid substitutions modifying the electrostatic properties of the A1 domain could impede heparin binding via loss of long-range and/or short-range electrostatic interactions.

Indeed, with regard to computations for variant molecules, the most striking alterations of the potentials are seen for mutants 6A, R571A/K572A/R573A, K643G/K644G, and 4G. If the the heparin−VWF interaction is considered to involve, first, long-range electrostatic interactions and, in a second step, short-range ionic interactions, the data reported in Figure 6 show that for most single variants the electrostatic contours are not altered as compared to the WT molecule. That is, a large electropositive contour covering part of the molecule is observed and runs from the α3 helix up to the α6 helix. The experimental results described in the previous paragraphs mean that none of the single replaced positively charged residues contributes significantly to the free energy of binding. This correlates well with the undisturbed contours of most single variants. The key difference between 6A and the R571A/K572A/R573A mutant comes from an enhanced electronegative contour around the α3 helix of mutant 6A, even though both mutants have reduced positive potentials around the N-terminus of the α3 helix. In mutant 6A, we see that the negative contour around the α3 helix is enhanced (Figure 6). Thus, this region could be involved in long-range and short-range interactions. For the K643G/K644G mutant and even more so for variant 4G, the electropositive contour is altered. This indicates that an appropriate distribution of charges is essential in attracting heparin at some distances and that some important direct contacts are probably lost. As seen in the next paragraph, these results help localize heparin on the surface of the A1 domain.

Proposed VWF−Heparin Models via Rigid Body Docking. The initial approach of the positively charged VWF A1 domain to a negatively charged heparin molecule should be guided by the asymmetry of the protein's electrostatic potential so that the regions with the most positive potentials should contact heparin first. Several orientations of heparin on the electropositive side of the A1 domain were generated and compared with the mutagenesis data. The three most electrostatically favorable orientations when a rigid heparin molecule is positioned onto the A1 domain are shown in Figure 7A. In one binding mode (orientation 1), the heparin long axis is oriented somewhat parallel to helix α3 with a strong contribution from charged residues located between positions 571 and 579. In another binding mode (orientation 2), heparin bridges the N-terminal area of the α3 helix with the C-terminal regions of the α5 and α6 helices. In the third orientation, heparin has mainly electrostatic interactions with the C-terminal regions of the α5 and α6 helices. The combination of a detailed evaluation of the A1 domain surface potentials and numerous experimental data, including the mutagenesis analysis presented here, led to the selection of orientation 2 as the most likely position of heparin at the surface of VWF (Figure 7B). Indeed, such a binding mode seems to be the only way to dock a relatively extended heparin molecule at the surface of the A1 domain in a manner that bridges the two electropositive clusters.

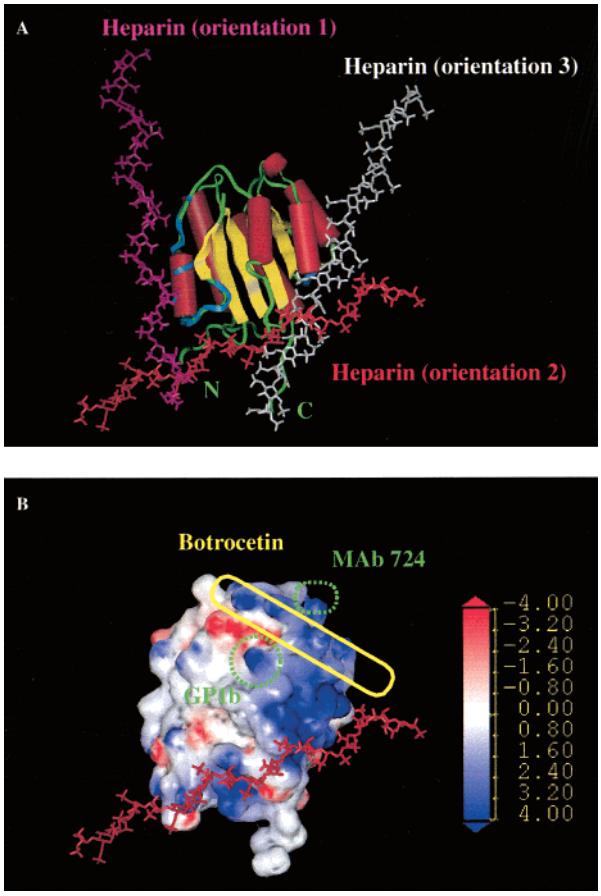

FIGURE 7: Proposed models of the VWF−heparin complex. (A) An 18-mer heparin molecule was docked interactively on top of the electropositive side of the A1 domain. Heparin and VWF were considered rigid molecules, and electrostatic interaction energies calculated according to Coulomb's law were investigated. The three lowest-energy values [heparin stick models colored magenta (orientation 1), red (orientation 2), and white (orientation 3)] are presented. (B) A theoretical model of the VWF−heparin complex is proposed on the basis of structural analysis of the A1 domain and known experimental data. The charge profile of the mainly electropositive side of the WT VWF A1 domain is mapped onto the molecular surface (regions of positive surface charge are represented in blue and regions of negative charge in red, while neutral is white). The scale at the right of the figure is in units of kT/e. Heparin could bend toward the botrocetin or mAb recognition site (see the Discussion).

DISCUSSION

The availability of structural information on the VWF A1 domain has helped design and rationalize experiments aimed at investigating molecular functions of VWF, for instance, to define important areas involved in the binding of platelet GPIb or botrocetin (*13*, *14*). Yet little information is available on the molecular mechanism governing VWF−heparin interaction, which may be relevant in understanding cardiovascular physiopathology. In an attempt to understand how heparin is positioned on the surface of the A1 domain, we decided to generate new data using both experimental and bioinformatics methodologies. We propose that heparin wraps around the N-terminal part of helix α3 toward the C-terminus of helix α5. Within this scenario, heparin would sit on top of two positively charged clusters consisting of some or all the following residues: one cluster of Arg^{571}, Lys^{572}, Arg^{573}, Arg^{578}, Arg^{579}, and Lys^{585} and another cluster of Lys^{642}, Lys^{643}, Lys^{644}, and Lys^{645}.

The affinity between heparin and VWF is moderate and is characterized by an apparent dissociation constant (K_d) of 3.78×10^{-7} M (*5*). Electrostatic forces contribute significantly to this reaction since a salt concentration of >200 mM NaCl affects the binding of heparin to VWF. Consequently, site-directed mutagenesis experiments aimed at probing the VWF−heparin interaction should essentially

involve neutralization of positively charged residues. Our experimental approach was thus a charged-to-neutral mutagenesis and involved residues located in each of the two relevant heparin binding sites. Fifteen different rVWF molecules containing one, two, three, four, or six mutations were created. Each of the mutant proteins was found to be similar to WT rVWF, with regard to its secretion, multimeric structure, and binding to several conformation-dependent mAbs directed against the A1 domain. These findings indicate that the conformation of the mutant's A1 domain was not damaged, in agreement with the fact that the substituted residues show 60−100% side chain accessibility to solvent and thus belong to regions where mutations are known to be structurally tolerated (*11*, *13*).

We have used a heparin coupling procedure where attachment of heparin to aminoethylagarose beads occurs only at the reducing terminal end of heparin, leaving most sulfate groups of heparin available for an interaction with VWF (*6*). This procedure was followed for screening heparin interaction with VWF in plasma from patients with VWD, and rVWF expressing the corresponding mutation (*26*, *32*). Under these conditions, we used large heparin quantities coupled to the beads to measure the level of binding independently of the multimeric VWF composition in plasma samples (*32*). The specificity of the VWF−heparin binding assay is demonstrated in this work by four independent arguments. (i) The first is a lack of binding with the ΔA1-rVWF, where all binding sites for heparin are missing (*7*). (ii) Soluble heparin, used as a competitor of solid-phase heparin for VWF binding, produced an IC_{50} value quite similar to that reported by Fujimura et al. (*5*) and a complete inhibition of binding at 0.5 mg/mL, while most authors studying VWF binding to heparin−Sepharose beads reported values between 1 and 7 mg/mL soluble heparin (*5*, *12*, *28*). (iii) We found that a 400-fold molar excess of unlabeled VWF over [^{125}I]VWF could completely inhibit binding of purified plasma-derived VWF to the same beads (data not shown). (iv) mAb 724, previously reported to block heparin binding to VWF (*23*), was able to inhibit heparin binding of WT, 6A, or 4G completely at a concentration of 5 μg/mL. When screening for a loss of binding among the 15 mutants, we obtained a decreased binding level of 40−60% for 6A, 4G, and K643G/K644G mutants. We confirmed this loss of binding by changing the amount of solid-phase heparin. Considering that decreasing the amount of solid-phase heparin results in a shift toward saturation of heparin by VWF, we found that the level of binding of the 6A and 4G mutants was decreased 10-fold compared to that of the WT.

Binding to GPIb was diversely affected, depending on the substitutions. In agreement with others (*12*, *15*, *33*), we found that several mutations, namely, R571A, R571A/K572A/R573A, and 4G, profoundly affected the ability of rVWF to bind GPIb in the presence of ristocetin. The substitution of four lysines, from position 642 to 645, with alanine was also reported to exhibit a decreased level of binding to GPIb in the presence of botrocetin (*12*, *33*). In addition, we found that the 6A variant exhibited a decreased level of binding to GPIb in the presence of ristocetin. In contrast to the loss of function, we found that R573A, R578A/R579A, and R578A/R579A/R585A exhibited a gain of function when binding to GPIb was assessed in the presence of low ristocetin concentrations, compatible with a type 2B phenotype. This finding confirms and extends previous data of others, indicating the key role of Arg^{578} (*31*).

To investigate heparin−VWF interactions, we combined experimental and computational approaches. All mutant proteins were recognized by several conformation-dependent mAbs in the same way as the WT, confirming that their 3D structure could not be significantly different from that of the WT. This observation indicated that a standard energy minimization protocol was appropriate for relaxing the WT and mutant structures. We expected to find regions of electropositive potentials around the A1 domain and indeed observed that this domain has an electropositive side or face (Figure 6). This face of the module bears most of the key functional sites of the protein (heparin, GPIb, and botrocetin binding). The attraction of heparin should be essentially guided by the asymmetry of the electrostatic potential so that the region with the most positive potentials contacts the polyanion first. Computation of the electrostatic potentials for the WT and mutants was carried out to correlate the extent of binding to heparin with the electropositivity of the mutants (i.e., mutations strongly affecting electropositive properties of the domain should not bind heparin very efficiently). Conceptually, when general information about protein−ligand interactions and more specific data on VWF−heparin binding are taken into account, this latter reaction may be considered to consist of three steps: (1) diffusion of heparin to its binding site on the A1 domain surface with electrostatic steering, (2) salt bridge and hydrogen bond formations together with van der Waals and hydrophobic contacts should maximize the interaction, and (3) at the same time, small conformational changes at the level of the protein and distortions of the heparin helix could take place.

In agreement with our experimental findings that only 4G, K643G/K644G, and 6A rVWF mutants have weaker interactions with heparin than WT rVWF, electrostatic calculations show that the extended electropositive contour present in the WT molecule displays some modifications for these three mutants. Although an extended nearly linear electropositive region is seen for mutant 4G, the isopotential contour is significantly altered. This indicates that the strong contribution to the binding of heparin comes from the four-lysine cluster, consistent with previous data about the importance of this site (*12*). The mutant K643G/K644G shows a significantly decreased level of binding to heparin, and its positive contour appears somewhat closer to that of mutant 4G than to that of mutant K642G/K645G. This suggests that residues 643 and 644 play a more important role in heparin binding than residues 642 and 645. In the 6A variant, negative potentials around the α3 helix are enhanced and may repulse heparin. The key difference between mutants 6A and R571A/K572A/R573A comes from the enhanced electronegative contour around the α3 helix of mutant 6A, although both mutants have reduced positive potentials around the N-terminus of the α3 helix. Thus, the mutant R571A/K572A/R573A can still interact with heparin, presumably through contacts at positions 578, 579, 585, and/or 642−645. Electrostatic data are thus in overall agreement with the experimental results and indicate, taking as example variants 6A and 4G, that disturbance of both long-range Coulombic interactions and short-range ionic contacts as a result of the mutations impedes proper binding of heparin. In contrast, single mutants bind to heparin in a fashion similar

to that of WT rVWF. This suggests that none of the substituted positively charged residues contributes significantly to the free energy of binding, but rather that the interaction requires multiple contacts, distributed on a relatively extended surface together with an overall electrostatic complementarity between the two molecules. This means that in the single mutants, diffusion of heparin to its binding site is not drastically damaged and that even if some hydrogen bonds or salt bridges are missing when the polyanion comes into close contact with the domain, other forces are sufficient to counterbalance the negative effects of the mutations. Also, as it is known that optimal heparin binding is achieved with a heparin fragment spanning 18 monosaccharides (*6*), it is very likely that numerous contacts spread over a relatively large surface have to take place at the same time to maintain the two molecules together. Therefore, it is not so surprising that a long heparin molecule starts to lose binding only when we introduce several mutations. At present, at least two main molecular mechanisms responsible for the binding of heparin to proteins have been described (*34*). In some systems, the binding of heparin is only weakly dependent on electrostatic forces, while in other situations (most common), the binding is mostly dependent on electrostatics. Clearly, in many cases, both electrostatic interactions and other forces (e.g., hydrophobic contacts, hydrogen bonds, and release of salt ions) contribute to binding. In all situations, one would expect that several key binding amino acids would be distributed on a relatively extended surface (e.g., 15 Å). Our data about the interaction of VWF with heparin are consistent with what is known about protein−heparin complex formation and correspond to a situation in which electrostatic forces play a key role during binding while other kinds of contacts are certainly important in further stabilizing the complex. However, the optimal recognition site for heparin at the surface of the A1 domain appears to be larger than in many systems and seems indeed to be extended over one entire face of the domain (see below).

Keeping in mind the above data and observations, we then searched for a model where the docking of heparin on the A1 surface would be compatible with (i) the length of heparin and (ii) the requirement for heparin to associate with each positively charged cluster. We positioned heparin at different locations on the surface of the domain and evaluated energies of electrostatic interaction between the two molecules. Although we used rigid docking approximation (e.g., heparin was assumed to behave as a stiff rod), we considered that simple interaction energy estimates, analyzed in conjunction with available experimental data, would lead to the selection of an overall reasonable structure for the complex. Three orientations were energetically favorable and are shown in Figure 7A. Obviously, if it had been computationally feasible to introduce flexibility, some local conformational changes could occur on both the protein and heparin. The most likely orientation for heparin was binding mode 2, consistent with the importance of residues 642−645 and 571−579. With such an orientation, an 18-mer heparin molecule could easily contact both regions (i.e., the distance between these two clusters is ∼30 Å). In orientation 1, heparin follows helix α3, but this location of the polyelectrolyte is unlikely because double or triple mutations of residues 571−573, 578 and 579, or 578, 579, and 585 have no or minor effects on heparin binding. Yet the interaction between VWF and heparin is dependent on electrostatic forces, and when these residues are mutated, there would be only a few positively charged amino acids remaining present on this helix. As such, this orientation is not compatible with experimental data. This area of the A1 domain is not very electropositive except for the N-terminal region of the α3 helix, and computed favorable interaction energies come essentially from contact between this part of the helix and heparin. Again, such a localized strong interaction between the two molecules could be possible; however, binding would not require the presence of at least 18-mer heparin, and mutations at positions 642−645 should have no effect on binding. In orientation 3, heparin essentially contacts helices α5 and α6 but could also bend toward the botrocetin binding site and the N-terminus of helix α3. Although this orientation is realistic, the fact that most of this surface is covered by botrocetin within the botrocetin−VWF complex but that heparin still binds the complex (*35*) suggests that orientation 2 is the most likely one. Crystal structure analysis of the A1 domain−botrocetin complex indicates that parts of the A1 domain α5 and α6 helices are covered by botrocetin while Lys^{599} (α4 helix, GPIb binding site) is still essentially accessible in the complex (*36*). In the absence of botrocetin and within our proposed binding mode (orientation 2), heparin could bend toward helices α5 and α6 and thus impair botrocetin−VWF complex formation. In the presence of botrocetin, sufficient contacts could still be provided by VWF region 571−579 and positively charged residues in the area of residues 642−645 or from botrocetin itself. Additional arguments in favor of orientation 2 come from data on mAb 724, which blocks VWF binding to botrocetin and which epitope maps to residues Lys^{660} and Arg^{663} (*15*, *23*). Interestingly, we found that either K660A or R663A displays a binding to heparin similar to that of WT, suggesting that none of these residues interacts individually with heparin, although we cannot exclude the possibility that a combined substitution could affect this function. The role of these residues in heparin binding is however unlikely as they seem to be covered by botrocetin when this latter is associated with VWF, while the interaction with heparin is not affected. Furthermore, each mutant with alanine or glycine substitution within the heparin binding regions shows normal binding to mAb 724, confirming that both clusters are located outside of the epitope. It has previously been reported that mAb 724 may induce conformational changes of the VWF A1 domain (*23*, *37*). This would point to an indirect mechanism through which mAb 724 inhibits VWF binding to heparin, in agreement with the present finding that this mAb exerts a comparable inhibitory effect toward WT, 6A, or 4G binding to heparin.

The current study provides new insights about the heparin binding site at the surface of the VWF A1 domain and proposes an overall orientation of heparin at the surface of the domain that is compatible with available experimental and structural data. This information may help in understanding whether heparin modulates negatively or positively the binding of VWF to GPIb, a subject that is still a matter of debate.

ACKNOWLEDGMENT

We thank Dr. J. E. Sadler for the kind gift of plasmids encoding K660A, R663A, and K667A and Dr. P. G. de Groot

for the gift of recombinant VWF-ΔA1. The technical support of Ghislaine Cherel is gratefully acknowledged.

REFERENCES

1. Sadler, J. E. (1998) *Annu. Rev. Biochem. 67*, 395−424.
2. Sobel, M., McNeill, P. M., Carlson, P. L., Kermode, J. C., Adelman, B., Conroy, R., and Marques, D. (1991) *J. Clin. Invest. 87*, 1787−1793.
3. Perrault, C., Ajzenberg, N., Legendre, P., Rastegar-Lari, G., Meyer, D., Lopez, J. A., and Baruch, D. (1999) *Blood 94*, 4186−4194.
4. Casu, B. (1989) *Ann. N.Y. Acad. Sci. 556*, 1−17.
5. Fujimura, Y., Titani, K., Holland, L. Z., Roberts, J. R., Kostel, P., Ruggeri, Z. M., and Zimmerman, T. S. (1987) *J. Biol. Chem. 262*, 1734−1739.
6. Baruch, D., Ajzenberg, N., Denis, C., Legendre, P., Lormeau, J. C., and Meyer, D. (1994) *Thromb. Haemostasis 71*, 141−146.
7. Sixma, J. J., Schiphorst, M. E., Verweij, C. L., and Pannekoek, H. (1991) *Eur. J. Biochem. 196*, 369−375.
8. Fretto, L. J., Fowler, W. E., McCaslin, D. R., Erickson, H. P., and McKee, P. A. (1986) *J. Biol. Chem. 261*, 15679−15689.
9. Mohri, H., Yoshioka, A., Zimmerman, T. S., and Ruggeri, Z. M. (1989) *J. Biol. Chem. 264*, 17361−17367.
10. Sobel, M., Soler, D., Kermode, J., and Harris, R. (1992) *J. Biol. Chem. 267*, 8857−8862.
11. Jenkins, P. V., Pasi, K. J., and Perkins, S. J. (1998) *Blood 91*, 2032−2044.
12. Kroner, P. A., and Frey, A. B. (1996) *Biochemistry 35*, 13460−13468.
13. Emsley, J., Cruz, M., Handin, R., and Liddington, R. (1998) *J. Biol. Chem. 273*, 10396−10401.
14. Celikel, R., Varughese, K. I., Madhusudan, Yoshioka, A., Ware, J., and Ruggeri, Z. M. (1998) *Nat. Struct. Biol. 5*, 189−194.
15. Matsushita, T., Meyer, D., and Sadler, J. E. (2000) *J. Biol. Chem. 275*, 11044−11049.
16. Hilbert, L., Gaucher, C., and Mazurier, C. (1995) *Blood 86*, 1010−1018.
17. Veyradier, A., Jumilly, A. L., Ribba, A. S., Obert, B., Houllier, A., Meyer, D., and Girma, J. P. (1999) *Thromb. Haemostasis 82*, 134−139.
18. Ribba, A. S., Hilbert, L., Lavergne, J. M., Fressinaud, E., Boyer-Neumann, C., Ternisien, C., Juhan-Vague, I., Goudemand, J., Girma, J., Mazurier, C., and Meyer, D. (2001) *Blood 97*, 952−959.
19. Deng, W. P., and Nickoloff, J. A. (1992) *Anal. Biochem. 200*, 81−88.
20. Lankhof, H., Wu, Y. P., Vink, T., Schiphorst, M. E., Zerwes, H. G., de Groot, P. G., and Sixma, J. J. (1995) *Blood 86*, 1035−1042.
21. Meyer, D., Zimmerman, T. S., Obert, B., and Edgington, T. S. (1984) *Br. J. Haematol. 57*, 597−608.
22. Pietu, G., Ribba, A. S., Cherel, G., Siguret, V., Obert, B., Rouault, C., Ginsburg, D., and Meyer, D. (1994) *Thromb. Haemostasis 71*, 788−792.
23. Christophe, O., Rouault, C., Obert, B., Pietu, G., Meyer, D., and Girma, J. P. (1995) *Br. J. Haematol. 90*, 195−203.
24. Obert, B., Tout, H., Veyradier, A., Fressinaud, E., Meyer, D., and Girma, J. P. (1999) *Thromb. Haemostasis 82*, 1382−1385.
25. Nishikubo, T., Christophe, O., Lavergne, J. M., Obert, B., Nonami, K., Takahashi, Y., Yoshioka, A., Meyer, D., and Girma, J. P. (1997) *Thromb. Haemostasis 77*, 174−182.
26. Rastegar-Lari, G., Ajzenberg, A., Ribba, A. S., Vereycken-Holler, V., Legendre, P., Villoutreix, B. O., Meyer, D., and Baruch, D. (2001) *Thromb. Haemostasis 86*, 1459−1465.
27. Schullek, J., Jordan, J., and Montgomery, R. R. (1984) *J. Clin. Invest. 73*, 421−428.
28. de Romeuf, C., and Mazurier, C. (1993) *Thromb. Haemostasis 69*, 436−444.
29. Honig, B., and Nicholls, A. (1995) *Science 268*, 1144−1149.
30. Mulloy, B., Forster, M. J., Jones, C., and Davies, D. B. (1993) *Biochem. J. 293*, 849−858.
31. Randi, A. M., Jorieux, S., Tuley, E. A., Mazurier, C., and Sadler, J. E. (1992) *J. Biol. Chem. 267*, 21187−21192.
32. Rastegar-Lari, G., Legendre, P., Ajzenberg, N., Warszawski, J., Meyer, D., and Baruch, D. (2000) *Hematol. J. 1*, 190−198.
33. Matsushita, T., and Sadler, J. E. (1995) *J. Biol. Chem. 270*, 13406−13414.
34. Hileman, L. E., Fromm, J. R., Weiler, J. M., and Linhardt, R. J. (1998) *BioEssays 20*, 156−167.
35. Andrews, R. K., Bendall, L. J., Booth, W. J., and Berndt, M. C. (1995) *Platelets 6*, 252−258.
36. Huizinga, E. G., Schouten, A., Romijn, R. A. P., Andrews, R., Berndt, M. C., Kroon, J., and Sixma, J. J. (2001) *Thromb. Haemostasis 80* (Abstract).
37. Depraetere, H., Ajzenberg, N., Girma, J. P., Lacombe, C., Meyer, D., Deckmyn, H., and Baruch, D. (1998) *Blood 91*, 3792−3799.

BI020044F